**Steel and Composite Structures**, *Vol. 33, No. 3* (*2019*) *389-402*
DOI: https://doi.org/10.12989/scs.2019.33.3.389


# Fragility assessment of shear walls coupled with buckling restrained braces subjected to near-field earthquakes

Hamid Beiraghi*

*Department of Civil Engineering*, *Mahdishahr Branch*, *Islamic Azad University*, *Mahdishahr*, *Iran*

(*Received March 8, 2019, Revised August 16, 2019, Accepted October 19, 2019*)

**Abstract.** Reinforced concrete walls and buckling restrained braces are effective structural elements that are used to resist seismic loads. In this paper, the behavior of the reinforced concrete walls coupled with buckling restrained braces is investigated. In such a system, there is not any conventional reinforced concrete coupling beam. The coupling action is provided only by buckling restrained braces that dissipate energy and also cause coupling forces in the wall piers. The studied structures are 10-, 20- and 30-story ones designed according to the ASCE, ACI-318 and AISC codes. Wall nonlinear model is then prepared using the fiber elements in PERFORM-3D software. The responses of the systems subjected to the forward directivity near-fault (NF) and ordinary far-fault (FF) ground motions at maximum considered earthquake (MCE) level are studied. The seismic responses of the structures corresponding to the inter-story drift demand, curvature ductility of wall piers, and coupling ratio of the walls are compared. On average, the results show that the inter-story drift ratio for the examined systems subjected to the far-fault events at MCE level is less than allowable value of 3%. Besides, incremental dynamic analysis is used to examine the considered systems. Results of studied systems show that, the taller the structures, the higher the probability of their collapse. Also, for a certain peak ground acceleration of 1 g, the probability of collapse under NF records is more than twice this probability under FF records.

**Keywords:** reinforced concrete walls; buckling restrained braces; coupling action; earthquake; near-field

## 1. Introduction

Shear walls play an important role in improving seismic behavior of building structures (Cao *et al*. 2003, Li *et al*. 2016, Gao *et al*. 2018, Qin *et al*. 2019). Coupled wall systems are traditionally one of the most widely-used lateral load-resisting systems for tall buildings. This configuration usually consists of two or more reinforced concrete (RC) shear walls in series, typically connected using RC beams at each floor level. Coupling action improves the overall building behavior by increasing the lateral stiffness and reducing the base moments that must be overcome by each wall (El-Tawil *et al*. 2010). Besides, due to the high stiffness of the RC walls, the coupling beams withstand great ductility demands. The aim of the design of a coupled wall is to resist the seismic loads, so that energy is dissipated through yielding of coupling beams along the height of the system and through flexural yielding at the wall base. Formation of the flexural plastic hinge at the wall base and flexural or shear hinges at the coupling beams is allowed in various codes (CSA Standard 2005, NZS 3101 2006, CEN EC8 2004).

As the coupling beams undergo nonlinear deformations during strong ground motions, they dissipate seismic energy, thus limiting large deformations associated with plastic hinging at the bases of the walls (Harries and McNeice 2006). The plasticity is distributed over a more extensive area of the structure with considerably higher energy dissipation compared to the energy dissipation of the cantilever walls (Harries *et al*. 2000). In a conventional coupled wall system, the accumulation of shear force from the coupling beams results in large axial forces in the wall piers. In coupled walls, lateral loads are resisted by a combination of axial compression/tension couple action in the wall pier and flexural moment of individual wall piers. For two coupled wall piers connected by coupling beams, the portion of the total moment resisted by a couple action of axial force generated in the wall piers is recognized as coupling ratio, CR. This ratio is proposed in Eq. (1) (Paulay and Priestley 1992)

$$\mathrm{CR} = \frac{\mathrm{T} * L}{\mathrm{M_{OTM}}} \tag{1}$$

Where T is the axial force in the wall pier generated due to lateral load, ‘L’ is the center to center distance of the wall piers and $\mathrm{M_{OTM}}$ is the total overturning moment at the base.

Generally, near-fault earthquake causes stronger effect on the structures. The severe implications of the near-fault (NF) effects in engineering design was recognized after the 1994 Northridge earthquake (Malhotra 1999, Makris and Chang 2000, MacRae *et al*. 2001). Although considerable achievements have been accomplished so far, there is still an obvious need to understand the behavior of buildings subjected to near-field events.

*Corresponding author, Ph.D., Professor,
E-mail: h.beiraghi@msh-iau.ac.ir


http://www.techno-press.org/?journal=scs&subpage=6
ISSN: 1229-9367 (Print), 1598-6233 (Online)

Generally, ground motions containing a pulse at the beginning of the velocity time history are classified as a particular category of the ground motions that cause unexpected damages to buildings. This type of motion, named pulse like ground motion, is usually observed at near-fault sites. Forward directivity effect is commonly considered as the reason why this issue happens. In this way, the direction of fault rupture and the direction of seismic slip on a fault are aligned with that of the site. Most of the energy in this kind of ground motion gathers in a narrow frequency band and produces high intensity velocity pulses that are oriented at the fault- normal direction. (Somerville *et al*. 1997, Somerville 2003, 2005, Spudich and Chiou 2008). In reinforced concrete wall buildings, the characteristics of forward directivity NF seismic ground motion lead to a larger seismic demand when compared with the ordinary far-field (FF) seismic ground motion (Beiraghi *et al*. 2016a-c). Forward directivity near-fault ground motions have been identified as the cause of severe demands in structures that can exceed the predicted demands calculated from the RSA procedure (Bertero *et al*. 1978, Anderson and Bertero 1987, Akkar *et al*. 2005, Baker 2007, Vafaei and Eskandari 2014, Alavi and Krawinkler 2004, Beiraghi 2018a-d).

In recent years, buckling-restrained braces (BRBs) are some of the recognized structural elements that have a good energy dissipation capability. In fact, BRBs are relatively new components that can prevent brace buckling in compression. They are designed to yield and dissipate energy during both tension and compression (Abdollahzadeh and Banihashemi 2013, Black *et al*. 2002, Aiken *et al*. 2002, Beiraghi 2017). In conventional steel braces, buckling of brace element reduces the efficiency of the element in compression, and the hysteretic behavior of braces deteriorates severely under strong seismic loads. In the BRBs, the main concept is to confine a steel core element so that it can yield in compression as well as tension.

In high seismic risk region, coupling beams are often designed using diagonal reinforcement, rather than conventional top and bottom longitudinal reinforcement. More ductility and good energy dissipation are recognized as the advantages of this type of reinforcing. (Paulay and Priestley 1992). Coupling action reduces the structure displacement during strong earthquakes and also decreases the loss intensity due to the inelastic deflections. Diagonally reinforced coupling beams improve the behavior of the system and protect coupling beams against shear failure (Fox *et al*. 2014). Despite these advantages, diagonally-reinforced coupling beams have significant drawbacks. The large depth and complexity of detailing required to achieve adequate ductility in the beams lead to increased construction costs and time. Besides, repairing of damaged beams after severe events is a difficult task.

Generally, the damage of conventional RC coupling beams during severe events is a challenging issue. Repairing such elements is relatively bothersome. In this article, the behavior of tall coupled RC walls subjected to NF and FF earthquakes is investigated. In these structures, the coupling mechanism is provided only by BRBs. BRBs dissipate energy and also cause coupling forces in the wall piers. The structure is designed according to the code procedures and the nonlinear model of the RC wall is then prepared using the fiber elements. The seismic responses of the structures corresponding to the inter-story drift demand envelope, wall piers' curvature ductility, coupling ratio subjected to the two types of mentioned records are compared at maximum considered earthquakes. Besides, Incremental Dynamic Analysis (IDA) predicts complete structural responses and performances by subjecting a properly defined structural model to a suite of ground motion records. The intensity of these ground motions increased gradually, using scale factors to capture the whole structural responses, ranging from elastic to nonlinear large displacement response until structural collapse. IDA method will be described in other section. However, few investigations have applied IDA process in RC wall systems, and to the author's knowledge, for RC walls coupled with BRB, IDA method has not been applied before. Therefore, IDA curves were developed for NF and FF records to assess the performance. Fragility curves at different limit states were then extracted and compared for NF and FF ground motions.

## 2. Design

The examined structures were 10, 20 and 30-story buildings with a typical floor height of 3.5 m. The systems consist of two RC walls that are coupled by BRBs using a zigzag pattern. Fig. 1 shows the general view of the considered structures. The case-study models are plane structures and the beams are steel materials. The nominal design yielding stress of the reinforcement bar and steel material of the beams are 400 and 370 MPa, respectively. The nominal strength of concrete was assumed to be 45 MPa. To design the assumed structures, ETABS software version 13.1.1 was used to create an elastic finite element model and to design the elements. A shell-type plate element was used to simulate the RC wall. This kind of element uses a triangular or quadrilateral formulation that combines separate membranes and plate-bending behaviors. Line elements were used to model the beams. Connection of the beam to the wall was of the pinned type and wall base connection was of the fixed type. In each story, the portions of the dead and live load carried by the wall were assigned to the wall. The appropriate mass portion of each story was assigned to mass center of the model. The design of the frames was based on the ASCE-7 and ACI318-11 (ACI 318 2011, ASCE 7 2010). The specifications of the designed structures are shown in Tables 1 and 2. Wall thickness is constant along the height. The BRB specification was identical in every 0.2 H. Vertical steel reinforcement distribution was uniform at each cross-section. The vertical reinforcement ratio was determined such that the nominal flexural strength in each level was greater than that of the design envelope. The amount of reinforcement ratio was considered constant for every 20% of height from the base. The calculated reinforcement ratio is shown in Table 2. The minimum vertical reinforcement ratio was 0.25% (ACI 3182011).

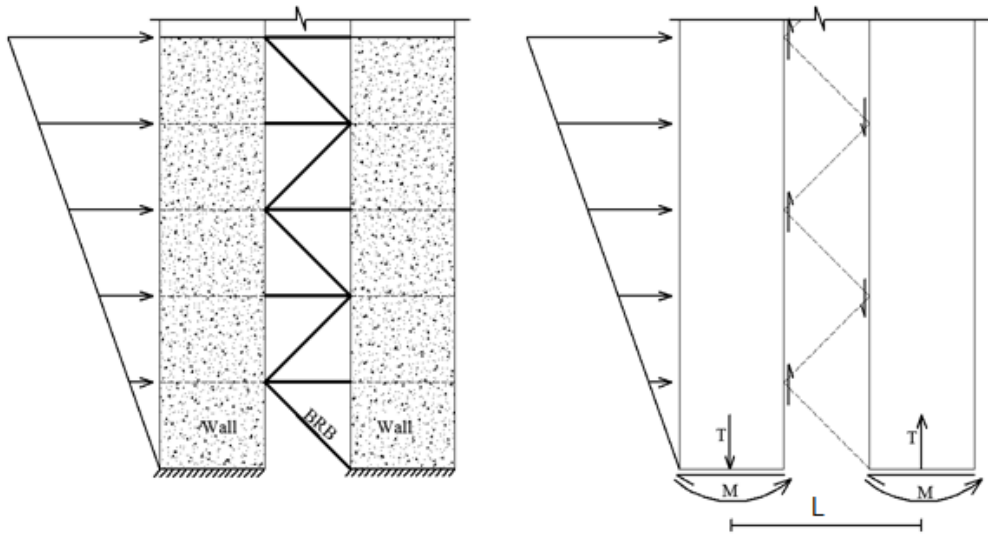


Fig. 1 General concept ohpgf the system: elevation of the coupled walls and BRBs; forces exerted on the system (both end of the beams and BRBs are pinned)

Table 1 Specification of the models

| | | 10ST | 20 ST | 30ST |
|---|---|---|---|---|
| Seismic weight corresponding to the system, W (ton) | | 1710 | 6040 | 15900 |
| P/(Ag.fc) at the wall base | | 0.056 | 0.078 | 0.097 |
| Wall thickness (m) | | 0.6 | 0.75 | 1.1 |
| Boundary zone height (No. of Story) | | 4 | 13 | 21 |
| Wall length (m) | | 3 | 4.5 | 6.5 |
| Design base shear/W (%) | | 11.8 | 6.9 | 6.0 |
| Effective response modification factor | | 5 | 5 | 4.56 |
| Coupling Ratio | **NF** | 61% | 55% | 52% |
| | **FF** | 61% | 55% | 53% |
| Period of natural vibration | **T1** | 0.89 | 2.23 | 3.38 |
| | **T2** | 0.235 | 0.49 | 0.68 |
| | **T3** | 0.109 | 0.22 | 0.31 |
| Modal participation mass ratio | **Mode 1** | 69 | 65 | 64 |
| | **Mode 2** | 17 | 19 | 19.5 |
| | **Mode 3** | 5.5 | 6 | 6 |
| | **Mode 4** | 3 | 3 | 3.2 |

To account for the effect of cracks on wall flexural stiffness, reduction factors for flexural stiffness were applied. A reduction coefficient of 0.5 was used for the effective moment of inertia of the RC wall cross-sections. This coefficient is in accordance with the stiffness reduction factors recommended in ACI 318-11 (Sections 8.8 and 10.10).

The natural free vibration periods, mode shapes and modal mass participation factors were determined using the response spectrum analysis (RSA) procedure. More than 90% of the modal participation mass ratio resulted from the first three translational modes of vibration. A 5% damping DBE level response spectrum was used in the RSA procedure (see Fig. 2). A response modification factor equal to eight (R = 8) was used to obtain the base shear demand from equivalent static procedure (ASCE/SEI 7-2010). The base shear force resulted from elastic RSA, Vt, was modified so that its quantity equaled 0.85 times the design equivalent static base shear force, V. ASCE 7 requires the forces to be multiplied by 0.85 V/Vt (ASCE/SEI 7-2010) when combined modal response of the base shear demand reduced by dividing by a design R factor (Vt) is less than 85% design equivalent static base shear force (V). This requirement controlled the design of 30-story model; therefore, effective response modification factor in the RSA procedure, Reff, is less than 5 in this case because the base shear from RSA is amplified to reach 85% design equivalent static base shear force (Table 1).

Table 2 Longitudinal reinforcement of the walls and core cross-section area of the BRBs

| | **Vertical reinforcement ratio of wall (%)** | | | **Core cross-section area of BRB ($cm^2$)** | | |
|---|---|---|---|---|---|---|
| Height range % | 10 ST | 20 ST | 30 ST | 10 ST | 20 ST | 30 ST |
| 0-20% | 2.24 | 2.34 | 2.22 | 88 | 150 | 300 |
| 21-40% | 1.3 | 1.39 | 1.29 | 88 | 140 | 230 |
| 41-60% | 0.87 | 1.05 | 1.01 | 88 | 100 | 140 |
| 61-80% | 0.56 | 0.77 | 0.79 | 75 | 88 | 120 |
| 81-100% | 0.32 | 0.34 | 0.38 | 47 | 75 | 100 |

To design BRBs, the current prescriptive codes were used (ASCE/SEI 7-2010). To calculate the specification of BRB components, axial forces calculated from the modal response spectrum analysis were reduced by the value of the response modification factor. The capacity of the braces

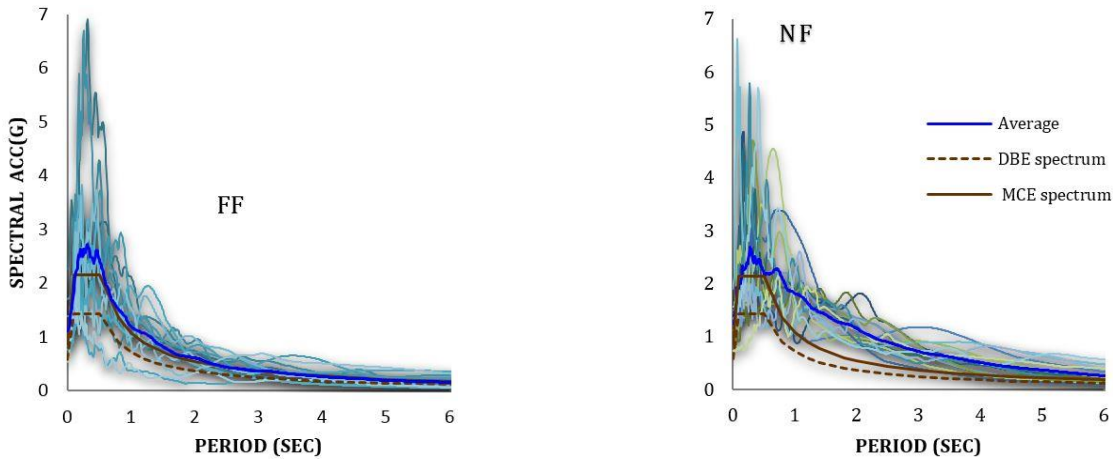


Fig. 2 MCE and DBE level spectra; individual and average spectra of considered NF and FF earthquakes

in tension and compression were considered as $\varphi A F_y$, where A is the cross section area of the brace element, φ = 0.9 and $F_y$ = 250 MPa.

## 3. Nonlinear model

Nonlinear dynamic responses of structures were studied in PERFORM-3D software (PERFORM-3D 2011). To model the RC walls, the fiber elements were utilized and the model is in 2D manner. Capability of these element types in efficient simulation of the shear walls behavior, under lateral forces, has been verified by the previous researchers (Beiraghi and Siahpolo 2016, Orakcal and Wallace 2006). According to Powell (2007), implementing one shear wall element over each story height is fundamentally sufficient to simulate the behavior of a shear wall. For the nonlinear model, the degradation factor is used to account for the stiffness and strength degradation (Ghodsi and Ruiz 2010). The beams were modeled with elastic elements. P-delta effect is considered in the calculations. Mass of each story is assigned to its center of the mass. Rigid diaphragms are used to equalize the horizontal displacement of the nodes of each floor. Each fiber cross section is comprised of the vertical steel and concrete fibers. For nonlinear fiber model of the wall, a confined concrete stress–strain based on the modified Mander model was assumed (Mander *et al*. 1988). Tensile strength of the concrete is ignored. The expected yield strength of the steel reinforcement was 1.17 times its nominal yield strength and the expected concrete fiber compressive strength was 1.3 times the specified strength used in the design procedure (LATBSDC 2011).

In the fiber element approach, it is important to use the effective plastic hinge length at the base of the wall models. For analyses purposes, the plastic-hinge length (lp) in the RC walls can be calculated from the following formula given by Paulay and Priestley (1992)

$$Lp = 0.2Lw + 0.03h \tag{2}$$

Where Lw is the RC wall length and h is the wall height. The height of the finite element used to model the plastic hinge shall not exceed the length, Lp, or the story height at the location of the critical section (LATBSDC 2011).

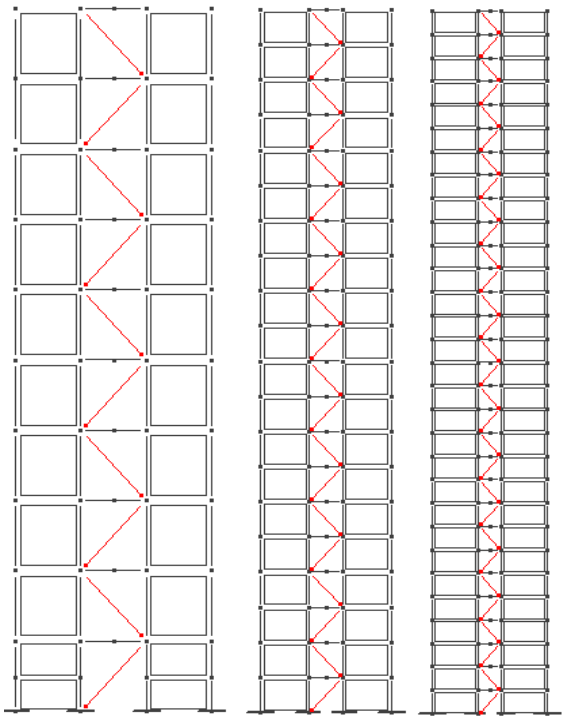

Fig. 3 Elevation view of the nonlinear models for 10-, 20- and hpg30-story structures in Perform-3D

Fig. 3 plots the elevation view of the nonlinear structural models. For the shear action of the fiber elements, linear response was assumed in the RC wall models. A typical value for the shear stiffness of the wall models is GcAg/10 to GcAg/20 as recommended by ATC72 (Applied Technology Council 2010). In the current research, GcAg/15 was used, where GcAg was the elastic shear stiffness.

BRBs have the capability of combined isotropic and kinematic hardening. The post-yield stiffness of BRBs in

tension is different from that in compression. The reason is the Poisson expansion effect and friction at the interface between the core and the restraining material. According to the AISC, the seismic behavior of BRBs including strain hardening is accounted with the compression strength and the strain hardening adjustment factors. Thus, the maximum compression forces from the brace are calculated as $R_y \omega \beta A F_y$, where $R_y$ = 1.1 accounts for the material over strength, ω = 1.25 considers the strain-hardening effect and β = 1.1 is the compression over-strength factor (Jones and Zareian 2013).

BRB element in the Perform-3D is a bar-type element that resists axial force only and has no resistance to torsional or bending forces (PERFORM-3D User guide 2006). The element contains two portions in series: a linear portion that is elastic and a nonlinear core portion capable of yielding.

### *3.1 Verification*

For a shear wall element in the PERFORM-3D, in-plane behavior in vertical direction is much more important than the transverse behavior. A fiber element may have inelastic behavior in bending and/or shear response. Transverse in-plane behavior of shear wall element is essentially elastic and secondary. When the steel fibers yield in a wall element and/or concrete fibers crack, the effective centroid axis shifts (PERFORM-3D 2011).

To verify the accuracy of the shear wall element, an experimental testing of a slender 4-story RC shear wall subjected to cyclic lateral loading is used (Thomsen and Wallace 2004). Capacity design was used to design this specimen to allow for flexural hinging at its base. For modeling, 5 nonlinear shear wall elements over the height (two elements for the first story and one element for the other stories) are implemented (PERFORM-3D 2006). Generally, the top displacement due to lateral loads is neither relatively sensitive to the mesh size nor to the number of material fibers (Orakcal and Wallace 2006).

An axial force of 0.07 Agfc, where Ag is the area of the wall cross-section, and fc is the concrete compression strength resulting from the test are applied to the specimen and held constant throughout the test duration, and cyclic lateral displacement is applied at the top of the wall. The height of the wall is 10 feet and the thickness is 4 inches and the length of the wall is 48 inches.

Fig. 4(a) compares the results of numerical and experimental hysteresis loops for the examined RC wall. The horizontal axis is the lateral drift at the top of the specimen.

The verification of the BRB elements was calibrated by a test result, considering the assumptions mentioned before. Load-deformation graph of BRBs has been illustrated in Fig. 4(b). The initial stiffness quantity was K0 and the first yield occurs at yield deformation Dy pertaining to Fy. Post-yield stiffness (KH) was 5% of the initial stiffness, up to the deformation of DU = 5 Dy. Maximum total strain in the brace, before the occurrence of negative stiffness was 2.8%.

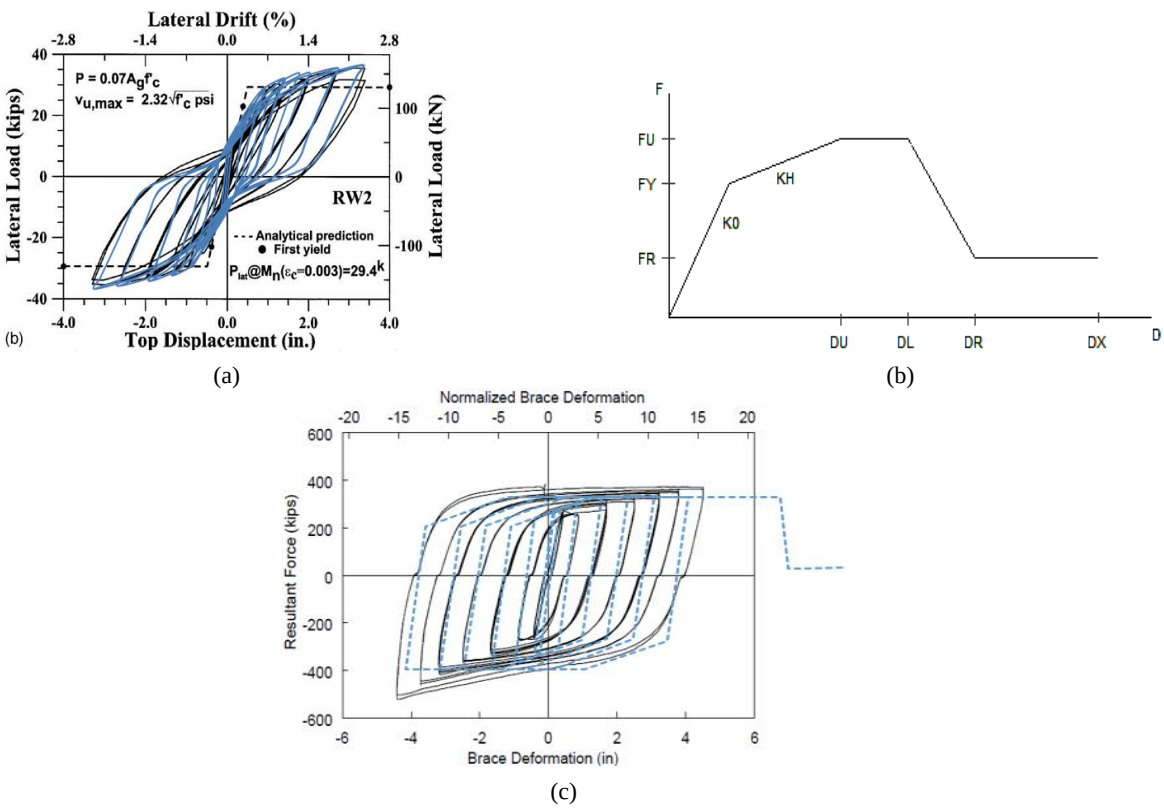


Fig. 4 (a) Hysteretic loops from numerical model by author (blue color) and from experimental wall tested by Orakcal and Wallace (2006); (b) General load-axial deformation action of the BRB; (c) Hysteretic loops of BRB from numerical model (dashed line by the author)

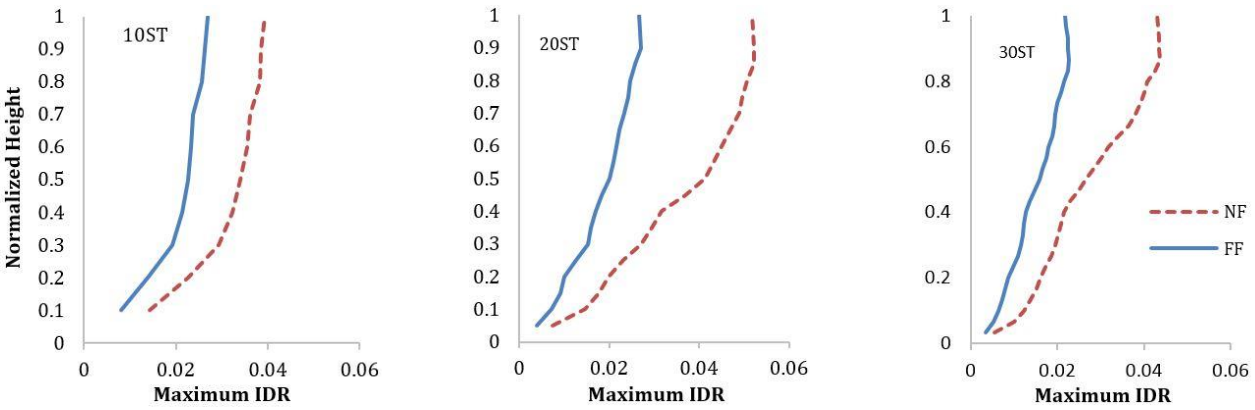


(a) (b) (c)

Fig. 5 Mean of inter-story drift ratio envelopes at MCE level earthquakes

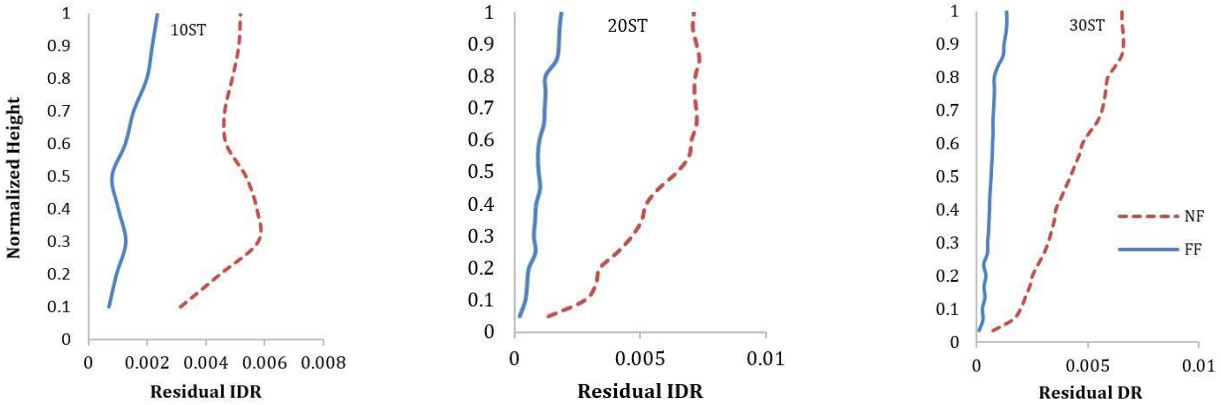


(a) (b) (c)

Fig. 6 Mean of residual inter-story drift ratio envelopes at MCE level earthquakes

With the assumed core length of 70% of the total total length, the maximum core strain will be 4% (DL) and fracture was assumed to happen when the core strain reached 4%. This method has been used by other researchers. To achieve numerical convergence after fracture, a minimum residual strength was used. The force-displacement hysteretic loops obtained from the numerical and experimental works, have been compared in Fig. 4(c). The general responses calculated from the numerical model and test program are approximately similar. The same approach described above is used for BRB elements in the studied models. As the specified yielding stress is 250 MPa, the corresponding yielding strain of the core material is 0.00125 and the expected yielding strain is 0.00138.

In this study, 0.15% Rayleigh damping is used for the first and third modes, in addition to 2.5% modal damping for all modes, as recommended by the computer program guidelines (Perform-3D 2006).

### *3.2 Ground motions*

Nonlinear time history analysis (NLTHA) requires use of appropriate earthquake records corresponding to maximum considered earthquake (MCE) or DBE ground motion levels. The MCE response spectrum graph is 1.5 times the DBE response spectrum graph (ASCE/SEI 7-2010). This study implements the nonlinear analysis for the considered systems subjected to the fault normal component of pulse-like near-fault and ordinary far-fault ground motions. For this purpose, a suite of 14 forward-directivity near-fault and 14 far-fault ground motions were selected from the ground motions set of FEMA P695 (2009). The time history of the records is obtained from the PEER NGA database. Also, these records are used in IDA. The specifications of the ground motion are taken from Beiraghi *et al*. (2016a) and the scaling procedure of the records was completed as per ASCE7.

## 4. Responses from NLTHA

Fig. 5 plots the mean maximum inter-story drift ratio MIDR, envelopes pertaining to the near-fault (NF) and far-fault (FF) records at MCE level. The vertical axis represents the normalized height. Maximum IDR occurs at the top of the 10-story structure and this issue occurs at the 0.85H in the 20- and 30-story structures. Maximum IDR obtained from the FF records is less than 3%. It is worth noting that LATBSDC declares that the average MIDR of a building subjected to a set of earthquake records at MCE level must be less than 3%. However, the MIDR envelope pertaining to the NF records for the 10- 20- and 30-story structures is 3.9,

5.2 and 4.3%, respectively. On average, the MIDR of the NF records is 4.5%, that is 1.5 times the allowable value.

Residual IDR is another index to assess the behavior of the structures. According to the LATBSDC, maximum allowable value for residual IDR at MCE level earthquake is 1%. Large residual IDR of the buckling restrained braced frames is one of the most recognized critical deficiencies of these systems. As it is demonstrated in Fig. 6, for all cases, the mean residual IDR envelope of the structure is less than the mentioned limit. Maximum RIDR of the 10- 20- and 30-story structures subjected to the FF records is 0.23, 0.18 and 0.14%. Subjected to the NF records, these values are 0.57, 0.73 and 0.66%, respectively. The maximum residual IDR demand obtained from NF events is approximately 3.5 times the corresponding value obtained from FF records. From the economy viewpoint, scholars believe that rebuilding is preferred to repairing when maximum residual IDR exceeds 0.5% (McCormick *et al*. 2008).

Mean of the structures' lateral displacement demand envelopes subjected to the NF and FF records at MCE level earthquake are plotted in Fig. 7. The horizontal axis is normalized by dividing the lateral displacement of each story by the total height of the structures and the vertical axis represents normalized height. On average, roof lateral displacement ratio of the systems subjected to NF records is approximately twice the corresponding value from FF earthquakes. Generally, as it is obvious from the Fig. 7, the system deformation mode tends to be in flexure; so, the slope of each displacement curve at the upper level of the structure is larger than the corresponding value at the lower levels.

Fig. 8 shows the mean curvature ductility demand envelope of the RC wall in the 10-, 20- and 30-story building subjected to MCE level earthquakes. Curvature ductility demand is an indicator of plasticity extension in the RC wall. The rotation demand measurement over each wall element was accomplished using rotation gauge elements in the Perform-3D computer program and the approximate curvature, $\Phi$, was calculated by dividing the rotation demand by the element height. Eq. (3) was used to obtain the yield curvature, $\Phi y$. This Equation was proposed by Paulay for rectangular RC walls (Paulay and Priestley 1992).

$$\Phi_y = \frac{1.8\varepsilon_y}{L_w} \tag{3}$$

Where $\varepsilon_y$ is the expected yield strain of reinforcement bars that is equal to 0.00234, and $L_W$ is the wall horizontal length. RC wall curvature ductility was calculated from $\Phi/\Phi_y$. It is assumed that the demand curvature is constant along an element. A limit value for the curvature ductility is 3.0 at which the concrete contribution to shear resistance

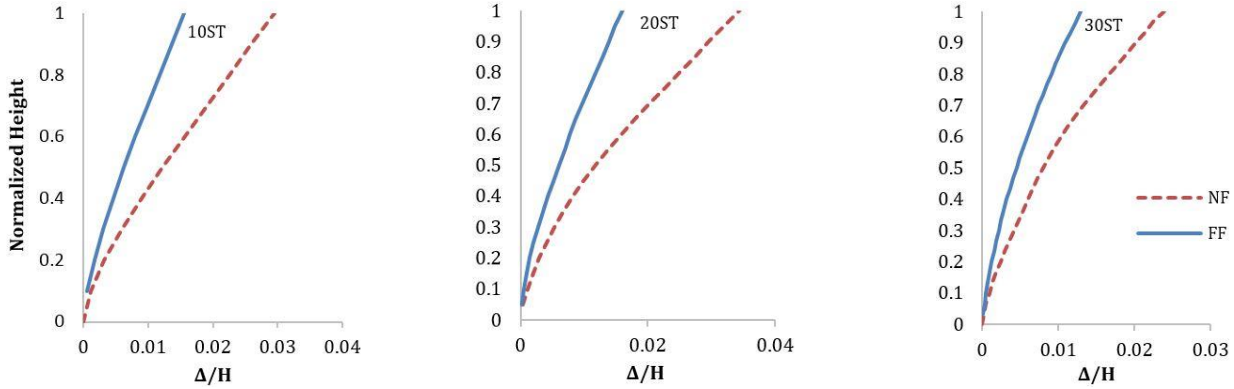


(a) (b) (c)

Fig. 7 Mean of normalized lateral displacement envelopes at MCE level earthquakes

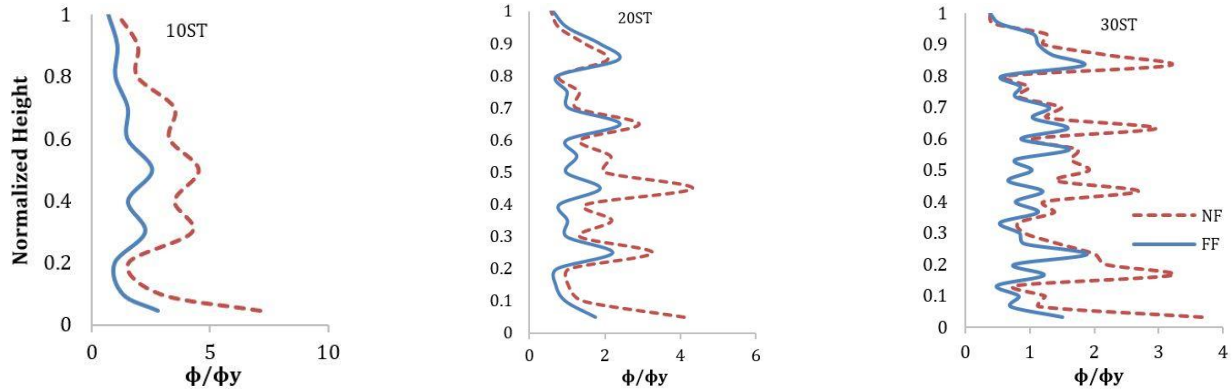


(a) (b) (c)

Fig. 8 Mean of curvature ductility envelopes pertaining to the wall piers at MCE level earthquakes

begins to reduce (Priestley *et al*. 1996, Fox *et al*. 2014).

According to the Fig. 8, for the NF events, greatest plasticity extension occurs at the base of the RC walls and the curvature ductility values are 7.1, 4.1 and 3.7 for the 10-, 20- and 30-story, respectively. In the 20- and 30-story structures subjected to the FF events, the maximum curvature ductility does not happen at the base, but the difference between the curvature ductility demand at the base and upper levels is slight. The maximum curvature ductility value pertaining to the FF events is less than 2.8. Consequently, the plasticity extension in the RC wall is slight in these events.

This value is below the upper limit of 3.0 mentioned above. In both NF and FF events, the plasticity extension in the upper region of the walls is moderate. In high RC core-wall structures in which the lateral force resistant system is just the RC wall, the plasticity extension in the upper region of the wall is critical (Beiraghi *et al*. 2016a, b), whereas in this study it is not considerable. Changes in longitudinal reinforcement ratio in the RC wall and changes in cross-section area of the BRBs affect local rising in the curvature ductility demand curve along the height of the structure. This issue is also affected by the zigzag arrangement of the BRBs. On average, the maximum curvature ductility demand calculated using NF records is approximately 2 times the corresponding demand value calculated using FF records.

Mean story shear demand envelopes of the structures subjected to the considered events at MCE level are represented in Fig. 9. Shear demand value in the horizontal axis has been divided by the total seismic weight of the structure (W) and the vertical axis represents normalized height. In each story, the contribution of the RC wall and BRBs in the shear force have been separated. Fig. 9 plots the contribution of BRBs and the wall for bearing the lateral shear load along the height. It is obvious that in each level of the structure, the shear force is carried by both RC wall and BRBs. At the lower levels, the shear contribution of the wall is considerably larger than that of the BRB.

The shear demand in each story of buildings subjected to the NF events is near the corresponding values obtained from using FF events. The reason is the plasticity extension in RC wall as well as BRBs along the height of the structures for both set of events. At the base of the 10-, 20- and 30-story structures, the shear contribution of the RC wall is approximately larger than 3, 7 and 8 times the contribution of the BRB. This ratio is larger for the taller structures, since designing process requires larger dimension for RC wall to fulfill the drift criteria. However, these ratios are reduced at the upper levels, but the ratio is also significant.

Fig. 10 shows the average envelope of the maximum

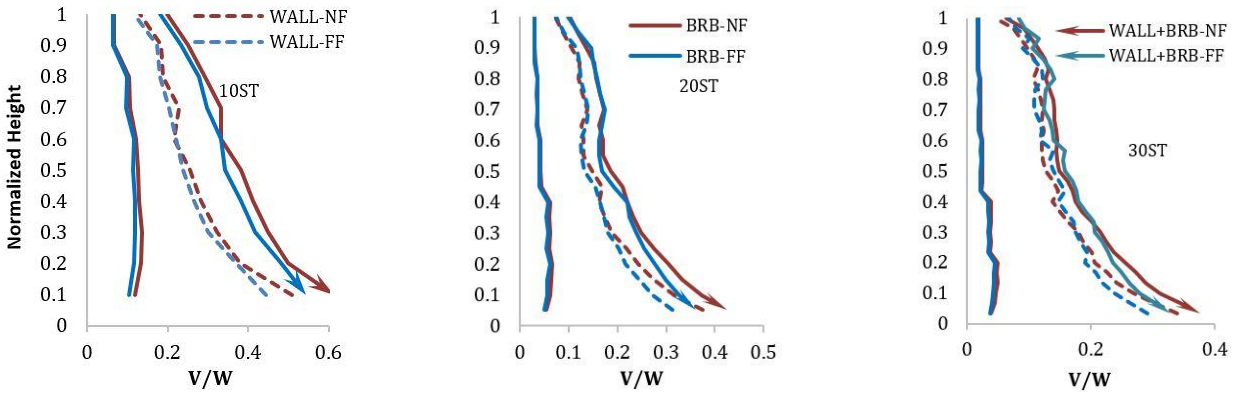


(a) (b) (c)

Fig. 9 Mean of normalized story shear envelopes as well as the contribution of walls and BRBs at MCE level earthquakes

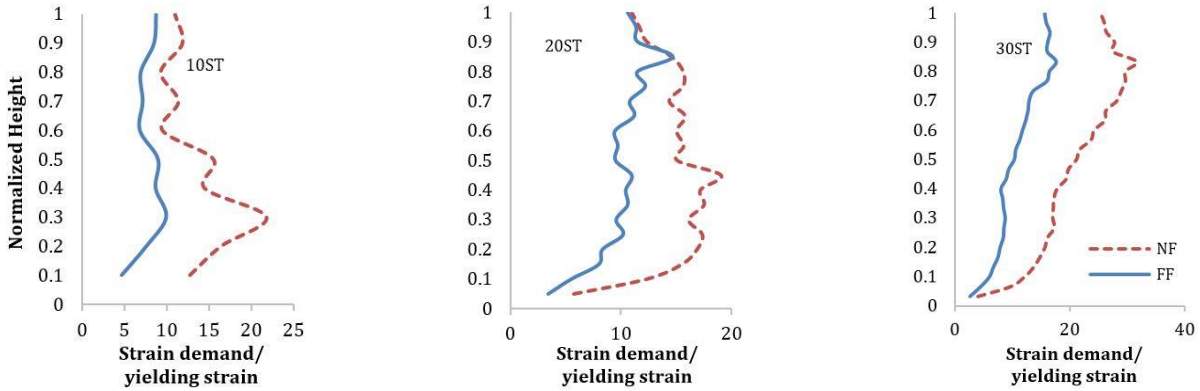


(a) (b) (c)

Fig. 10 Mean of strain demand envelopes divided by yielding strain in the core of BRBs at MCE level earthquakes

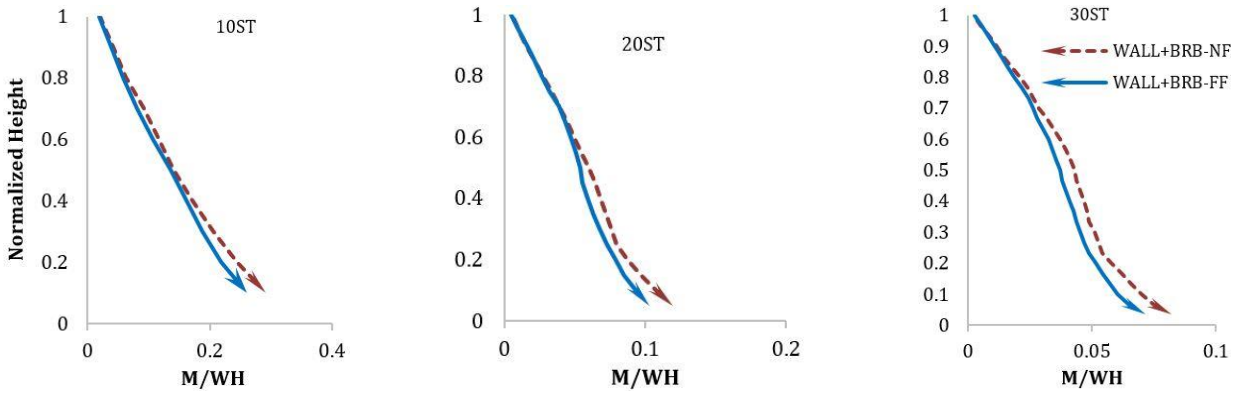


(a) (b) (c)

Fig. 11 Mean of normalized overturning moment envelopes at MCE level earthquakes

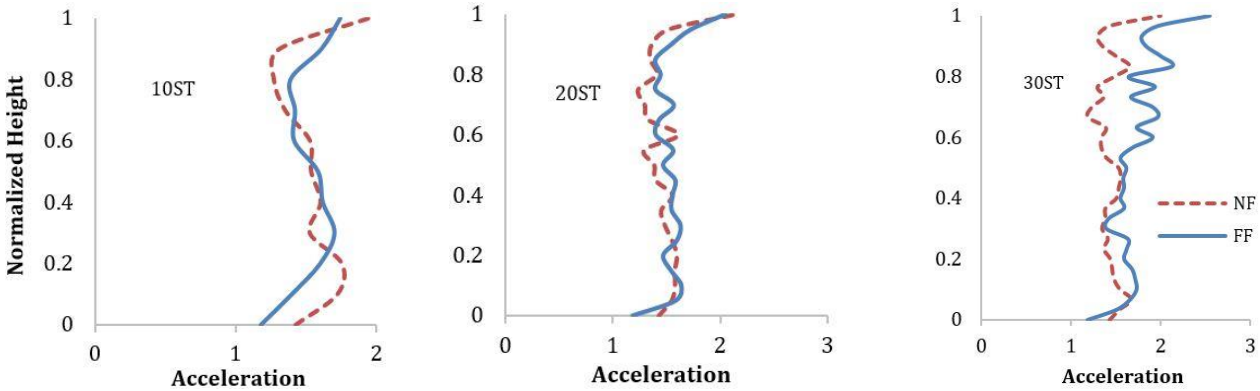


(a) (b) (c)

Fig. 12 Mean story acceleration envelopes at MCE level earthquakes

axial strain ratio in the core of the BRBs along the height at MCE level earthquakes. Horizontal axis is the ratio of strain demand to yielding strain quantity of the core. The local rising in the strain ratio demand curve of buckling restrained braced frames is because of the change in the BRB properties along the height and also because of zigzag arrangement of BRBs. Typically, the maximum strain ratio of BRB occurs in upper region and its level is higher for taller buildings. The general trend of the graphs pertaining to the NF and FF events is similar. For FF earthquakes, the mean maximum BRB strain ratios for 10-, 20-, 30-story structures are approximately 10, 14 and 17, respectively. Whereas for the NF records, these values will be respectively 22, 19 and 31. On average, the maximum strain ratio in the BRBs pertaining to the NF events is 1.75 times the corresponding value pertaining to the FF events. It is worth mentioning that the acceptance criteria for the strain ratio of the BRBs according to the ASCE 41-13 is almost13.3 and the maximum strain of the BRB core shall not exceed 2.5%. In this research, for each structure, the average of maximum strain of BRB core subjected to the FF events was less than 2.5% and in each case of 10-, 20- and 30-story structures subjected to NF events, this value was 3.2, 2.8 and 4.5% respectively.

The mean story overturning moment demand envelope along the height of the structures at MCE level earthquakes has been shown in Fig. 11. The moment envelopes have been normalized by the product of the total seismic weight and height of the buildings. Commonly, in the taller buildings, the moment envelope diagram shows a little inflation at the mid-height, because of the effect of higher vibration modes. On average, the difference between the base moment demand resulted from NF and FF events is less than 10%, which is because of over strength and strain hardening effect after the plastic hinges formation.

Some nonstructural elements are sensitive to acceleration, like parapets, suspended ceilings, ducts, boilers, chiller tanks, etc.. Fig. 12 shows the stories horizontal acceleration demand envelops at MCE level earthquakes over the structure height. The mean base acceleration for the NF earthquake is nearly 1.15 times the mean base acceleration for the FF earthquakes. For both sets of records, acceleration envelope at the upper levels exceeds the base acceleration, and this issue is more severe for the FF records. In all cases, the maximum acceleration occurs at the roof level.

For the examined coupled walls subjected to seismic loads, the coupling ratio can be defined as

$$\mathrm{CR} = \frac{\mathrm{Max}(\mathrm{T(t)} * \mathrm{L})}{\mathrm{Max}(\mathrm{M_{OTM}(t)})} \tag{4}$$

Where T(t) is axial load in the wall piers generated due to ground motion during time history of earthquake, 't' is the time, $M_{OTM}(t)$ is total overturning moment at the base of system and 'L' is the center to center distance of the wall piers. The coupling ratio quantity corresponding to the NF and FF records were approximately identical (see Table 1). The reason is the plasticity extension in wall pier as well as in almost all the BRBs subjected to both record sets. For taller buildings, the coupling ratio value is reduced. It was demonstrated that for taller buildings, larger axial strain in the BRBs was generated. Consequently, it appears that in taller buildings the axial stress of BRB increases by slow rate and so axial force of the wall pier increases slowly. This issue is due to post yielding slopes of the force-deformation curve corresponding to the BRB. Thus, the numerator of Equation cannot compensate for the overturning moment of denominator like before, so the coupling ratio decreases. On average, the coupling ratio of the systems is approximately 56%. This value is near the quantity that has been reported for conventional planar coupled RC walls by other researchers (Fox *et al*. 2014).

## 5. IDA process

Incremental Dynamic Analysis (IDA) is a useful method that thoroughly investigates structural performance subjected to seismic loads. In an IDA process, the system is subjected to a set of earthquake records of increasing intensity. Using IDA has widely been extended and considered as an effective method for the structural performance of buildings subjected to earthquake loads (Vamvatsikos and Cornell 2002).

To apply an IDA procedure for a selected earthquake records, the recorded accelerogram is scaled to different levels of intensity by multiplying various coefficients. At first, the multiplying factor is so small that the structure remains in linear elastic range and increases gradually, until either structural instability occurs, or the calculated inter-story drift demand becomes extremely large. Finally, a number of curves named IDA, depict the parameterized selected responses versus the earthquake record intensity levels. Generally, a large number of non-linear time history analyses are required to create IDA curves as explained comprehensively by Vamvatsikos and Cornell (Vamvatsikos and Cornell 2002). IDA is a useful analysis method for building performance assessment, adopted in the latest FEMA documents such as FEMA P-58 (FEMA P-58 2012), FEMA P-695 (FEMA P695 2009), etc.

### *5.1 Performance measure*

A performance measure is a way to quantify the outcomes associated with the response of a building subjected to strong ground motions, in such a way that are meaningful to decision-makers. Researchers and standards have used a number of different performance measures. In order to distinguish the expected performance of buildings, structural engineers have commonly used a series of well-known standard performance levels, like Operational, Immediate Occupancy, Life Safety, and Collapse Prevention. These performance levels are described by allowable ranges of strength and deformation demands on structural and nonstructural components. For example, descriptions for Slight, Moderate, Extensive, and Complete structural damage states for some building types have been provided by the HAZUS MR4's (National Institute of Building Sciences 2004).

Seismic behavior of a system in IDA procedure is commonly represented through the relationship between Damage Measure (DM) of a system and Intensity Measure (IM) parameter of the earthquake record. Parameters of DM and IM depend on the purpose of study and require careful definitions. Lateral displacement and inter-story drift are recognized as the most usual DMs in seismic study of structures (Kruep 2007). This research focuses on structural assessment of RC wall systems coupled by BRBs. The maximum inter-story drift ratio was then selected as the DM. IMs of ground motion excitations can be considered by a variety of parameters such as PGA, PGV or 5% damped first-mode spectral acceleration Sa (T1,5%), etc. Sa (T1,5%) as well as PGA are proper and effective IMs and researchers have used both parameters in their studies. Therefore, in the current research, PGA was adopted as the IM.

Inter-storey drift ratio is a widely recognized DM in numerical studies that can define the limit state for each performance level. Performance limit states based on inter-storey drift were adopted from previous standards/ recommendations. The values are 0.5%, 1% and 2% for IO, LS and CP performance levels of concrete walls, and 1%, 1.5% and 2% for braced steel frames, respectively (ASCE/SEI 41-13 2014, FEMA 356 2000). Generally, there is not an agreement about the CP performance level. It is believed that CP performance limit state depends on the onset of strength deterioration, and this issue depends on the ductility capacity of structural elements. In this study, these limit states are also adopted from FEMA 356. It should be noted that for each story, according to LATBSDC, and in order for collapse prevention evaluation, the average of absolute values of the maximum inter-story drift ratios from a suite of analyses shall not exceed 3%. Therefore, this limit state is also considered in present research. A story drift limit of 0.03 have been judged proper by experts in recent tall building projects at collapse prevention level. Generally, it is believed that, up to this story drift, structures with suitable yielding mechanisms and proper detailing will perform well (without considerable loss of strength), and that nonstructural components will not pose a major life safety hazard (LATBSDC 2011).

Eventually, IDA was performed on the three considered numerical models. The obtained IDA curves for 10, 20- and 30-story building subjected to FF and NF records are plotted in Figs. 13 and 14, respectively. These IDA curves were obtained via a series of nonlinear time history analyses, when each selected earthquake record was applied structural models at increasing intensity. The lowest scale factor value belongs to the PGA of the record scaled to 0.1 g and gradually increased by a 0.1 g step, until building models collapsed or underwent large IDR. Generally, the

dispersion of the responses pertaining to the NF record set is less than that of the FF record set. Besides, it can be concluded that for the considered systems subjected to both NF and FF record sets, the taller the structure, the smaller the tolerable maximum PGA. On average, the maximum tolerable PGA pertaining to the FF records is larger than that of NF records.

### *5.2 Fragility analysis*

IDA results can help to evaluate the seismic vulnerability of the examined systems, by calculating fragility curves derived for a building at each limit state. Fragility curves graphically display the probability of exceeding a limit state at a selected intensity of earthquake excitation, represented as

$$F = P(DL|IM) \tag{5}$$

Where, IM is the defined ground motion intensity measure and DL is the performance limit state. P is the probability of exceeding a determined limit state.

In the current research, data points IM = x (i.e., PGA) pertaining to the 14 IDA curves corresponding to each defined limit state were assumed to be log-normally distributed (i.e., Ln(x) is normally distributed). So the probability of exceeding a damage level (DS) can be determined as

$$P(\leq DL) = \Phi\left(\frac{Ln(x) - \theta}{\beta}\right) \tag{6}$$

Where $P(\leq DL)$ is the probability that a ground motion with IM = x will cause the structure to exceed the assumed limit state. Φ is the standard normal cumulative distribution function. $\theta$ and $\beta$ are the mean and the standard deviation of Ln(x) ($\beta$ sometimes known as the dispersion of IM). Equation 1 demonstrates that the IM values of ground motions corresponding to a given limit state for a structure are log normally distributed and this is a widely recognized assumption confirmed by a number of researchers (e.g., Ibarra and Krawinkler 2005). For the considered buildings at the different limit states pertaining to 0.5, 1, 1.5, 2 and 3% of maximum IDR, fragility curves are drawn comparatively in Fig. 15. In general, for the whole IDR threshold, difference between the fragility curves subjected to NF and FF records is significant. Besides, for taller building, the fragility curve is almost more critical. For example, for 30-St system, for probability of 50% exceeding the 2% IDR a PGA equal to 0.66 g and 0.8 g is calculated for NF and FF records, respectively, and

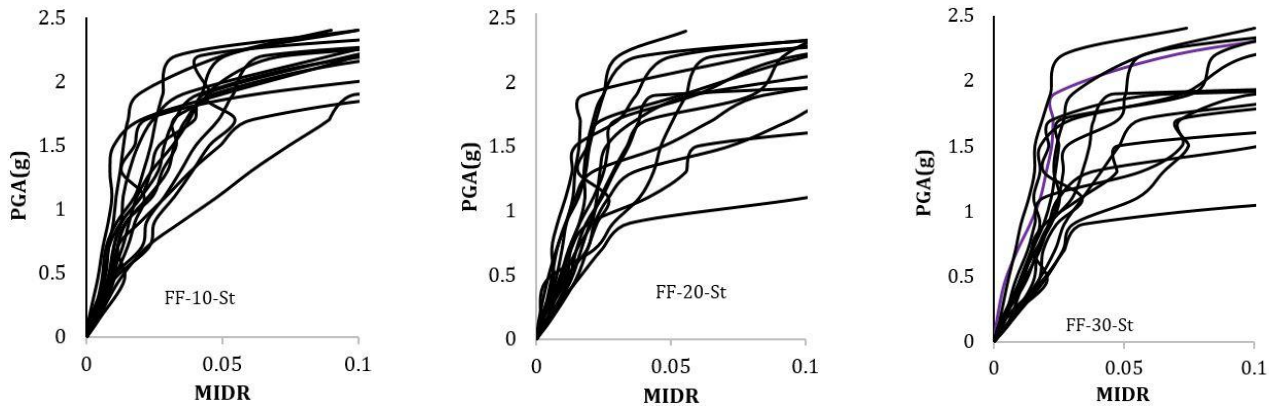


Fig. 13 IDA curves for 10, 20- and 30-story building subjected FF records

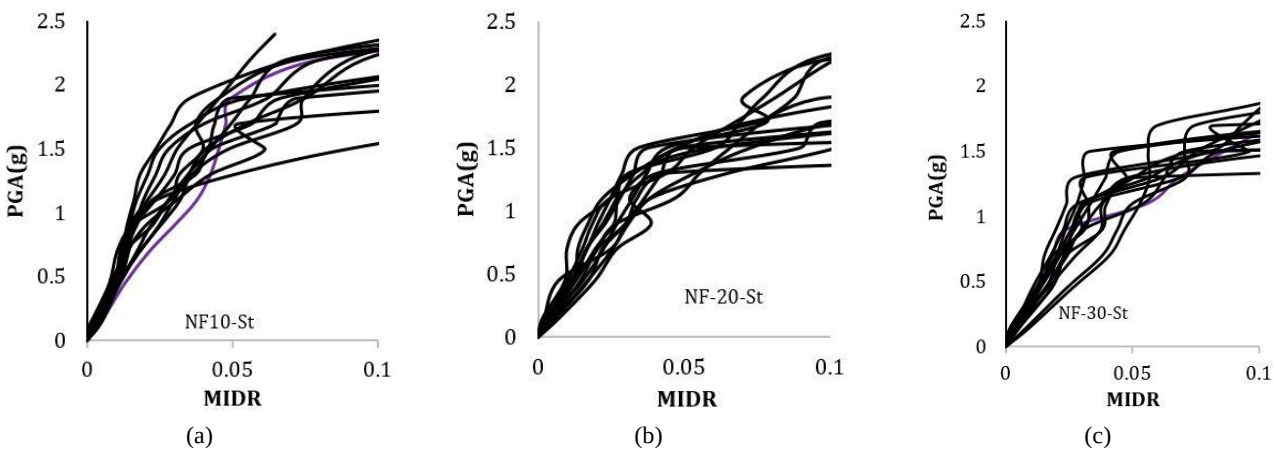


Fig. 14 IDA curves for 10, 20- and 30-story building subjected to NF and FF records

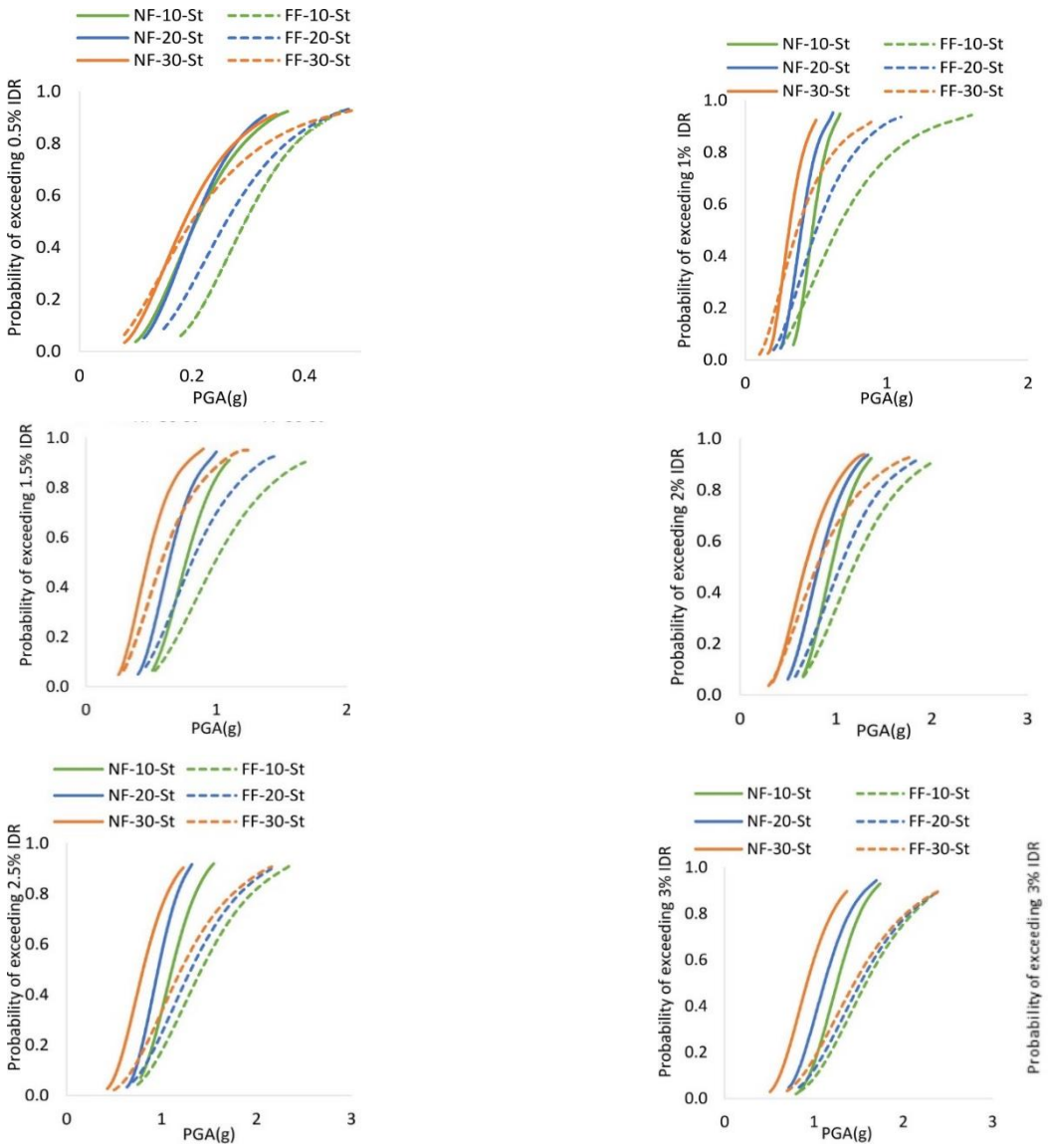


Fig. 15 Fragility curves at different limit states pertaining to 0.5, 1, 1.5, 2 and 3% maximum IDR for examined models

these quantities in 10–St system are 0.93 g and 1.17 g, respectively. It is worth to note that the design PGA for the models is 0.57 g. Results show that for the systems under investigation, and for examined levels of earthquakes, the taller the structure, the higher the probability of their collapse Also, for a certain peak ground acceleration of 1 g, the probability of collapse under NF records is more than twice this probability under FF records.

## 6. Conclusions

In this article, the behavior of the RC walls coupled with BRBs under both the ordinary FF and forward directivity NF events was investigated. The considered tall structures were designed using the RSA procedure. The nonlinear model of the RC wall was prepared using the fiber elements. The records were scaled to conform MCE level earthquakes. NLTHA procedure was implemented by applying the FF and NF earthquake records and the responses of structure were investigated. Mean quantity of maximum IDR envelopes pertaining to the FF records is less than the allowable 3% limit. However, on average, this quantity pertaining to the NF records is 4.5%, that is 1.5 times the allowable value. In both NF and FF events, the plasticity extension in the upper region of the RC wall is moderate. The maximum curvature ductility value of the RC wall pertaining to the FF events is less than 2.8. Consequently, the plasticity extension in the whole wall is slight. Except the base region, on average, the maximum curvature ductility demand subjected to NF events is 3.7 that is almost a moderate value. Generally, the maximum curvature ductility demand calculated using NF records is approximately twice the corresponding demand value calculated using FF records. The shear demand in each story of buildings subjected to the NF events is near the corresponding values obtained from using FF events. The reason is the plasticity extension in RC wall as well as BRBs along the height of the structures for both sets of events.

At the lower levels, the shear contribution of the wall is considerably larger than shear contribution of the BRB. However, this difference is reduced at the upper levels. On average, the maximum strain in the BRBs pertaining to the NF events is 1.75 times the corresponding value pertaining to the FF events. According to the ASCE 41-13, the maximum strain of the BRB core shall not exceed 2.5%. For the considered systems in this research, subjected to the FF events, this value was less than 2.5% and, subjected to NF events, this value is near 4.5% for 30-story structure. On average, the coupling ratio of the considered systems is approximately 56%.

In general, difference between the fragility curves subjected to NF and FF records is significant. Besides, for taller building, the fragility curve is almost more critical .For example for 30-St system, for probability of 50% exceeding the 2% IDR a PGA equal to 0.66 g and 0.8 g is calculated for NF and FF records, respectively, and these quantities in 10–St system are 0.93 g and 1.17 g, respectively. Therefore, it can be generalized from the result that for the considered systems, the taller the structure, the bigger the collapse probability. In the end, it is an appropriate idea to use RC walls coupled with BRBs to control the seismic behavior of the building during sever ground motions. Replacing the BRBs after sever events is almost an easy task.

## References


Abdollahzadeh, G. and Banihashemi, M. (2013), "Response modification factor of dual moment-resistant frame with buckling restrained brace (BRB)", *Steel Compos. Struct., Int. J.*, **14**(6), 621-636. https://doi.org/10.12989/scs.2013.14.6.621

ACI 318-11 (2011), Building code requirements for structural concrete and commentary, ACI Committee 318; Farmington Hills, MI, USA.

Aiken, I.D., Mahin, S.A. and Uriz, P. (2002), "Large-scale testing of buckling-restrained braced frames", *Proceedings of Japan Passive Control Symposium, Tokyo Institute of Technology*, Japan, pp. 35-44.

AISC (2010), Seismic provision for structural steel buildings, American Institute of Steel Construction; Chicago, IL, USA.

Akkar, S., Yazgan, U. and Gulkan, P. (2005), "Drift estimates in frame buildings subjected to near-fault ground motions", *J. Struct. Eng.*, **131**(7), 1014-1024. https://doi.org/10.1061/(ASCE)0733-9445(2005)131:7(1014)

Alavi, B. and Krawinkler, H. (2004), "Behavior of moment-resisting frame structures subjected to near-fault ground motions", *Earthq. Eng. Struct. Dyn.*, **33**(6), 687-706. https://doi.org/10.1002/eqe.369

Anderson, J.C. and Bertero, V.V. (1987), "Uncertainties in establishing design earthquakes", *J. Struct. Eng.*, **113**(8), 1709-1724. https://doi.org/10.1061/(ASCE)0733-9445(1987)113:8(1709)

Applied Technology Council (2010), ATC-72: Modeling and Acceptance Criteria for Seismic Design and Analysis of Tall Buildings, ATC, Redwood City, CA, USA.

ASCE/SEI 41-13 (2014), Seismic evaluation and rehabilitation of existing buildings, American Society of Civil Engineers; Reston, VA, USA.

ASCE/SEI 7-2010 (2010), Minimum Design Loads for Buildings and Other Structures, American Society of Civil Engineers; Reston, VA, USA.

Baker, J.W. (2007), "Quantitative classification of near-fault ground motions using wavelet analysis", *Bull. Seismol. Soc. Am.*, **97**(5), 1486-1501. https://doi.org/10.1785/0120060255

Beiraghi, H. (2017), "Earthquake effects on the energy demand of tall reinforced concrete walls with buckling-restrained brace outriggers", *Struct. Eng. Mech., Int. J.*, **63**(4), 521-536. https://doi.org/10.12989/sem.2017.63.4.521

Beiraghi, H. (2018a), "Energy demands in reinforced concrete wall piers coupled by buckling restrained braces subjected to near-fault earthquake", *Steel Compos. Struct., Int. J.*, **27**(6), 703-716. https://doi.org/10.12989/scs.2018.27.6.703

Beiraghi, H. (2018b), "Energy Dissipation of Reinforced Concrete Wall Combined with Buckling-Restrained Braces Subjected to Near- and Far-Fault Earthquakes", *Iran J. Sci. Technol. Trans. Civil Eng.*, **42**(4), 345-359. https://doi.org/10.1007/s40996-018-0109-0

Beiraghi, H. (2018c), "Reinforced concrete core-walls connected by a bridge with buckling restrained braces subjected to seismic loads", *Earthq. Struct., Int. J.*, **15**(2), 203-214. https://doi.org/10.12989/eas.2018.15.2.203

Beiraghi, H. (2018d), "Near-fault ground motion effects on the responses of tall reinforced concrete walls with buckling-restrained brace outriggers", *Scientia Iranica, Transact. A, Civil Eng.*, **25**(4), 1987-1999. https://doi.org/10.24200/sci.2017.4205

Beiraghi, H. and Siahpolo, N. (2016), "Seismic assessment of RC core-wall building capable of three plastic hinges with outrigger", *Struct. Des. Tall Special Build.* https://doi.org/10.1002/tal.1306

Beiraghi, H., Kheyroddin, A. and Kafi, M.A. (2016a), "Forward directivity near-fault and far-fault ground motion effects on the behavior of reinforced concrete wall tall buildings with one and more plastic hinges", *Struct. Des. Tall Special Build.*, **25**(11), 519-539. https://doi.org/10.1002/tal.1270

Beiraghi, H., Kheyroddin, A. and Kafi, M.A. (2016b), "Energy dissipation of tall core-wall structures with multi-plastic hinges subjected to forward directivity near-fault and far-fault earthquakes", *Struct. Des. Tall Special Build.*, **25**(15), 801-820. https://doi.org/10.1002/tal.1284

Beiraghi, H., Kheyroddin, A. and Kafi, M.A. (2016c), "Effect of record scaling on the behavior of reinforced concrete core-wall buildings subjected to near-fault and far-fault earthquakes", *Scientia Iranica, Transact. A. Civil Eng.*, **24**(3), p. 884.

Bengar, H.A. and Aski, R.M. (2016), "Performance based evaluation of RC coupled shear wall system with steel coupling beam", *Steel Compos. Struct., Int. J.*, **20**(2), 337-355. https://doi.org/10.12989/scs.2016.20.2.337

Bertero, V., Mahin, S. and Herrera, R. (1978), "A seismic design implications of near-fault San Fernando earthquake records", *Earthq. Eng. Struct. Dyn.*, **6**(1), 31-42. https://doi.org/10.1002/eqe.4290060105

Black, C., Makris, N. and Aiken, I. (2002), "Component testing, stability analysis and characterization of buckling-restrained brace", Report No. PEER-2002/08; Pacific Earthquake Engineering Research Center, University of California, Berkeley, CA, USA.

Cao, W.L., Xue, S.D. and Zhang, J.W. (2003), "Seismic performance of RC shear walls with concealed bracing", *Adv. Struct. Eng.*, **6**(1), 1-13. https://doi.org/10.1260/136943303321625685

CEN EC8 (2004), Design of Structures for Earthquake Resistance, European Committee for Standardization; Brussels, Belgium.

CSA Standard A23.3-04 (2005), Design of Concrete Structures, Canadian Standard Association; Rexdale, Canada.

El-Tawil, S., Harries, K.A., Fortney, P.J., Shahrooz, B.M. and Kurama, Y. (2010), "Seismic design of hybrid coupled wall systems: State of the art", *J. Struct. Eng.*, **136**(7), 755-769. https://doi.org/10.1061/(ASCE)ST.1943-541X.0000186

Federal Emergency Management Agency (2000), Prestandard and Commentary for the Seismic Rehabilitation of Buildings, FEMA 356.

FEMA P-58 (2012), Seismic Performance Assessment of Buildings, Volume 1 – Methodology, Federal Emergency Management Agency; Washington D.C., USA.

FEMA P695 (2009), Quantification of Building Seismic Performance Factors (ATC-63 Project), Federal Emergency Management Agency; Washington D.C., USA.

Fox, M.J., Sullivan, T.J. and Beyer, K. (2014), "Capacity design of coupled RC walls", *J. Earthq. Eng.*, **18**, 735-758. https://doi.org/10.1080/13632469.2014.904255

Gao, D., You, P., Zhang, L. and Yan, H. (2018), "Seismic behavior of SFRC shear wall with CFST columns", *Steel Compos. Struct., Int. J.*, **28**(5), 527-539. https://doi.org/10.12989/scs.2018.28.5.527

Ghodsi, T. and Ruiz, J.A.F. (2010), "Pacific earthquake engineering research/seismic safety commission tall building design case study", *Struct. Des. Tall Special Build.*, **19**(2), 197-256. https://doi.org/10.1002/tal.542

Ghorbanirenani, I., Tremblay, R., Léger, P. and Leclerc, M. (2012), "Shake table testing of slender rc shear walls subjected to eastern north america seismic ground motions", *J. Struct. Eng.*, **138**(12), 1515-1529. https://doi.org/10.1061/(ASCE)ST.1943-541X.0000581

Harries, K.A. and McNeice, D.S. (2006), "Performance-based design of high-rise coupled wall systems", *Struct. Des. Tall Special Build.*, **15**, 289-306. https://doi.org/10.1002/tal.296

Harries, K.A., Gong, B. and Shahrooz, B.M. (2000), "Behavior and design of reinforced concrete, steel, and steel-concrete coupling beams", *Earthq. Spectra*, **16**(4), 775-800.

Ibarra, L.F. and Krawinkler, H. (2005), *Global Collapse of Frame Structures under Seismic Excitations*, John A. Blume Earthquake Engineering Center, Stanford, CA, USA, 324.

Jones, P. and Zareian, F. (2013), "Seismic response of a 40-storey buckling-restrained braced frame designed for the Los Angeles region", *Struct. Des. Tall Special Build.*, **22**(3), 291-299. https://doi.org/10.1002/tal.687

Kruep, S.J. (2007), "Using incremental dynamic analysis to visualize the effects of viscous fluid dampers on steel moment frame drift", Master's Thesis; Virginia Polytechnic Institute and State University, Blacksburg, VA, USA.

LATBSDC (2011), An alternative procedure for seismic analysis and design of tall buildings located in the Los Angeles region, Los Angeles Tall Buildings Structural Design Council.

Li, Y.F., Huang, C.L., Lin, C.T. and Hsu, T.H. (2016), "A study on the high seismic performance of RC structural walls under reversed cyclic loading", *Adv. Struct. Eng.*, **15**(7), 1239-1252. https://doi.org/10.1260/1369-4332.15.7.1239

MacRae, G.A., Morrow, D.V. and Roeder, C.W. (2001), "Near-fault ground motion effects on simple structures", *J. Struct. Eng. ASCE*, **127**, 996-1004. https://doi.org/10.1061/(ASCE)0733-9445(2001)127:9(996)

Makris, N. and Chang, S.P. (2000), "Response of damped oscillators to cycloid pulses", *J. Eng. Mech. ASCE*, **126**, 123-131. https://doi.org/10.1061/(ASCE)0733-9399(2000)126:2(123)

Malhotra, P.K. (1999), "Response of buildings to near-field pulse-like ground motions", *Earthq. Eng. Struct. Dyn.*, **28**, 1309-1326. https://doi.org/10.1002/(SICI)1096-9845(199911)28:11<1309::AID-EQE868>3.0.CO;2-U

Mander, J.B., Priestley, M.J.N. and Park, R. (1988), "Theoretical stress-strain model for confined concrete", *ASCE J. Struct. Eng.*, **114**(8), 1804-1826. https://doi.org/10.1061/(ASCE)0733-9445(1988)114:8(1804)

McCormick, J., Aburano, H., Ikenaga, M. and Nakashima, M. (2008), "Permissible residual deformation levels for building structures considering both safety and human elements", *Proceedings of the 14th World Conference Earthquake Engineering*, Beijing, China, Paper No. 05-06-0071.

National Institute of Building Sciences (2004), Direct physical damage – general building stock, HAZUS-MH Technical manual, Chapter 5, Federal Emergency Management Agency; Washington D.C., USA.

NZS 3101 (2006), New Zealand Standard, Part 1 — The Design of Concrete Structures, Standards New Zealand; Wellington, New Zealand.

Orakcal, K. and Wallace, J.W. (2006), "Flexural Modeling of reinforced Concrete Walls-Experimental Verification", *ACI Struct. J.*, **103**(2), 196-206.

Paulay, T. and Priestley, M. (1992), *Seismic Design of Reinforced Concrete and Masonry Buildings*, Wiley, New York, NY, USA.

PERFORM-3D (2006), Nonlinear Analysis and Performance Assessment for 3D Structures, V.4, User Guide, Computers and Structures, Inc.; Berkeley, CA, USA.

PERFORM-3D (2011), Nonlinear Analysis and Performance Assessment for 3D Structures, V.4.0.3. Computers and Structures, Inc.; Berkeley, CA, USA.

Powell, G. (2007), *Detailed example of a tall shear wall building using CSI's Perform 3D nonlinear dynamic analysis*, Computers and Structures Inc., Berkeley, CA, USA.

Priestley, M.J.N., Seible, F. and Calvi, G.M. (1996), *Seismic Design and Retrofit of Bridges*, Wiley, New York, NY, USA.

Qin, Y., Shu, G., Zhou, X., Han, J. and He, Y. (2019), "Height-thickness ratio on axial behavior of composite wall with truss connector", *Steel Compos. Struct., Int. J.*, **30**(4), 315-325. https://doi.org/10.12989/scs.2019.30.4.315

Simpson, Gumpertz, & Heger, Inc. (2009), *Detailed Design Write up for BRBF building*, San Francisco, CA, USA.

Somerville, P.G. (2003), "Magnitude scaling of the near fault rupture directivity pulse", *Phys. Earth Planet. In.*, **137**(1), 201-212. https://doi.org/10.1016/S0031-9201(03)00015-3

Somerville, P.G. (2005), "Engineering characterization of near fault ground motion", *Proceedings of 2005 New Zealand Society for Earthquake Engineering Conference*, Taupo, New Zealand, 8 p.

Somerville, P.G., Smith, N.F., Graves, R.W. and Abrahamson, N.A. (1997), "Modification of empirical strong ground motion attenuation relations to include the amplitude and duration effects of rupture directivity", *Seismol. Res. Lett.*, **68**(1), 199-222. https://doi.org/10.1785/gssrl.68.1.199

Spudich, P. and Chiou, B.S.J. (2008), "Directivity in NGA earthquake ground motions: Analysis using isochrone theory", *Earthq. Spectra*, **24**(1), 279-298. https://doi.org/10.1193/1.2928225

Thomsen, J.H. and Wallace, J.W. (2004), "Displacement-based design of slender reinforced concrete structural walls—experimental verification", *J. Struct. Eng.*, **130**(4), 618-630. https://doi.org/10.1061/(ASCE)0733-9445(2004)130:4(618)

Vafaei, D. and Eskandari, R. (2014), "Seismic response of mega buckling-restrained braces subjected to fling-step and forwarddirectivity near-fault ground motions", *Struct. Des. Tall Special Build.* https://doi.org/10.1002/tal.1205

Vamvatsikos, D. and Cornell, C.A. (2002), "Incremental dynamic analysis", *Earthq. Eng. Struct. Dyn.*, **31**(3), 491-514. https://doi.org/10.1002/eqe.141

*CC*